Click Here for Full Article

# A silent $M_w$ 4.7 slip event of October 2006 on the Superstition Hills fault, southern California

Meng Wei,[1] David Sandwell,[1] and Yuri Fialko[1]

[1] During October 2006, the 20-km-long Superstition Hills fault (SHF) in the Salton Trough, southern California, slipped aseismically, producing a maximum offset of 27 mm, as recorded by a creepmeter. We investigate this creep event as well as the spatial and temporal variations in slip history since 1992 using ERS-1/2 and Envisat satellite data. During a 15-year period, steady creep is punctuated by at least three events. The first two events were dynamically triggered by the 1992 Landers and 1999 Hector Mine earthquakes. In contrast, there is no obvious triggering mechanism for the October 2006 event. Field measurements of fault offset after the 1999 and 2006 events are in good agreement with the interferometric synthetic aperture radar data indicating that creep occurred along the 20-km-long fault above 4 km depth, with most of the slip occurring at the surface. The moment released during this event is equivalent to a $M_w$ 4.7 earthquake. This event produced no detectable aftershocks and was not recorded by the continuous GPS stations that were 9 km away. Modeling of the long-term creep from 1992 to 2007 creep using stacked ERS-1/2 interferograms also shows a maximum creep depth of 2–4 km, with slip tapering with depth. Considering that the sediment thickness varies between 3 km and 5 km along the SHF, our results are consistent with previous studies suggesting that shallow creep is controlled by sediment depth, perhaps due to high pore pressures in the unconsolidated sediments.

## 1. Introduction

[2] Aseismic creep refers to fault slip that does not produce seismic radiation. Both geological and geodetic observations document evidence of creep along many fault segments in California [*Steinbrugge and Zacher*, 1960; *Tocher*, 1960; *Nason*, 1971; *King et al.*, 1973; *Burford and Harsh*, 1980; *Prescott et al.*, 1981; *Schulz et al.*, 1982; *Wesson*, 1988; *Burgmann et al.*, 2000; *Lyons et al.*, 2002; *Lyons and Sandwell*, 2003]. Fault creep releases elastic strain and reduces the hazard from future earthquakes [*Mavko*, 1982; *Burgmann et al.*, 2000; *Toda and Stein*, 2002; *Schmidt et al.*, 2005; *Fialko*, 2006; *Lienkaemper et al.*, 2006], making it an important part of seismic hazard estimation.

[3] The Superstition Hills Fault (SHF) is located on the southern extent of the San Jacinto fault zone (Figure 1). This fault has a well documented history of surface creep, most of which is triggered by nearby earthquakes as seen in 1951, 1968, 1987, 1989, 1992 and 1999 [*Allen et al.*, 1972; *Hudnut and Sieh*, 1989; *Bodin et al.*, 1994; *Rymer et al.*, 2002]. The 1987 $M_s$ 6.6 earthquake was the largest event on

this segment in 300 years and was extensively investigated in a number of seismic and geodetic studies [*Bilham*, 1989; *Boatwright et al.*, 1989; *Hudnut and Clark*, 1989; *Hudnut et al.*, 1989a; *Hudnut et al.*, 1989b; *Hudnut and Sieh*, 1989; *Klinger and Rockwell*, 1989; *Lindvall et al.*, 1989; *Mcgill et al.*, 1989; *Sharp*, 1989; *Sharp et al.*, 1989; *Sharp and Saxton*, 1989; *Williams and Magistrale*, 1989]. During the 11 years before the 1987 earthquake, the average rate of surface creep was 0.5 mm/a [*Louie et al.*, 1985]. A creepmeter installed after the 1987 earthquake [*Bilham and Behr*, 1992] showed afterslip at an average rate of 28 mm/a consisting of episodic creep events superimposed on a slow quasi-steady slip of 2.4 mm/a through 1991. No creepmeter data are available between 1991 and 2004. A new creepmeter was installed in March 2004 and recorded steady creep at a rate of 1.35 mm/a through October 2006. Dextral creep events occurred on 11 August 2005 with an amplitude of 0.5 mm and on 20 January 2006 with an amplitude of 0.35 mm. Starting on 3 October 2006, creep events occurred with an amplitude of more than 27 mm over the next 14 days, with 85% of the amplitude manifested in the first 3 days (Figure 2). For the 2006 creep event there was no obvious triggering event. The 2006 creep event was not detected seismically nor was it observed on the closest continuous GPS station 9 km from the fault. A better understanding of the poorly recorded creep history of the SHF has implications not only for the earthquake hazard assessment in the Imperial Valley area, but also for the

---

[1]Institute of Geophysics and Planetary Physics, Scripps Institution of Oceanography, University of California, San Diego, La Jolla, California, USA.
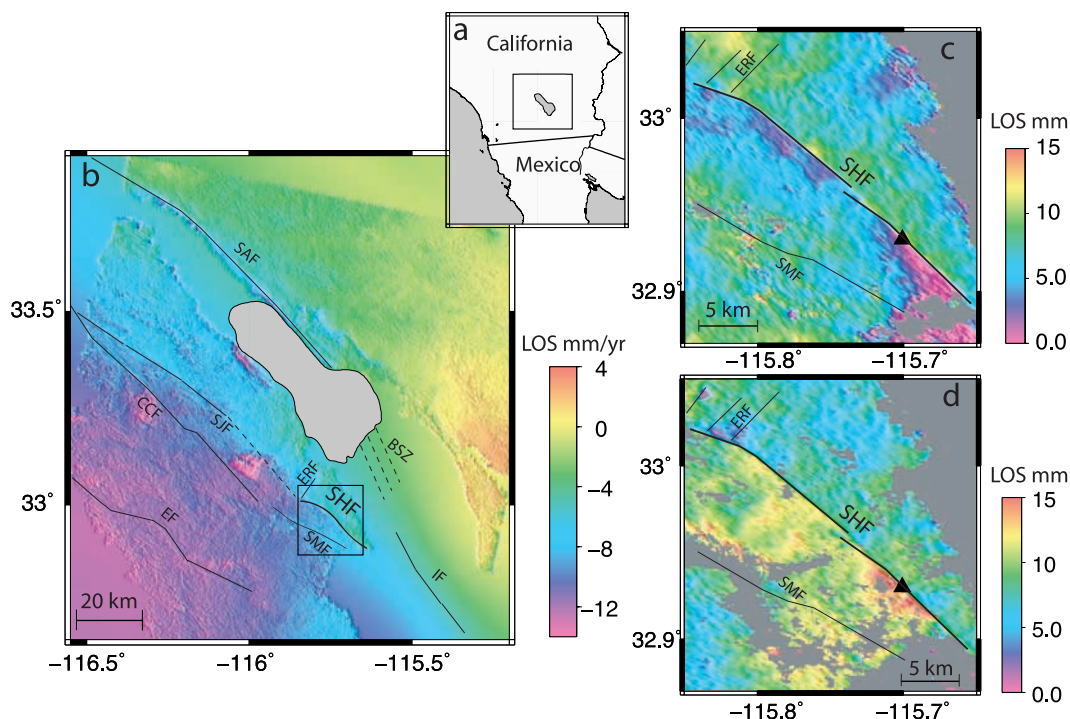
**Figure 1.** (a) Research area in southern California. The square box is the location of Figure 1b. (b) Stacked 13 interferograms of 15 years' ERS-1/2 data (track 356, frame 2925/2943). The square box on the midbottom is the area of Figures 1c and 1d. (c) Stacked seven descending interferograms of Envisat data (track 356, frame 2943) that span the 2006 creep event. The black lines trace the Superstition Hills fault (SHF), the Elmore Ranch fault, and the Superstition Mountain fault. The black triangle is the location of a creepmeter. (d) Stacked two ascending interferograms of Envisat data (track 77, frame 657) that span the 2006 creep event. Fault names are abbreviated as follows: SAF, San Andreas Fault; SJF, San Jacinto fault; EF, Elsinore fault; SHF, Superstition Hills fault; SMF, Superstition Mountains fault; IF, Imperial fault; ERF, Elmore Ranch fault; BSZ, Brawley seismic zone; CCF, Coyote Creek fault.

general understanding of the physical mechanisms of fault slip and the depth-dependent transition from velocity strengthening to velocity weakening in the shallow part of the seismogenic zone [*Marone and Scholz*, 1988].

[4] While creepmeters can provide excellent temporal coverage of fault slip [*Bilham et al.*, 2004], they do not reveal the spatial variations in displacement that are needed to infer the along-strike and downdip variations in slip. Field measurements of the surface offset can provide information on along-strike variations due to creep events [*Rymer et al.*, 2002] although they are not always performed or are often incomplete. It is possible that the ground cracking can be distributed across a fault zone so that a portion of slip can be overlooked. Moreover, neither field measurements nor sparse GPS measurements (>10 km spacing) can record the variations in cross-fault displacement that are needed to infer the slip distribution with depth [*Lorenzetti and Tullis*, 1989; *Thatcher*, 1990; *Savage and Lisowski*, 1993; *Fialko et al.*, 2001; *Simpson et al.*, 2001; *Wyss*, 2001; *Malservisi et al.*, 2005; *Schmidt et al.*, 2005; *Funning et al.*, 2007]. Repeat-pass radar interferometry [*Massonnet and Feigl*, 1998] is a valuable tool for measuring spatial variations in fault slip at length scales greater than about 50 m. The main limitations of the interferometric synthetic aperture radar (InSAR) are the poor temporal coverage (e.g., given large repeat interval) and lack of phase correlation in vegetated areas [*Rosen et al.*, 1996]. Fortunately, a large section of the SHF is located in arid desert and hence well correlated in the interferometric images (Figure 1). To our knowledge, this is the first time that both extensive field measurements and InSAR interferograms are available for multiple creep events in this area.

[5] There are three goals of this article. The first is to estimate the magnitude and depth of creep along the SHF associated with the October 2006 creep event. The creepmeter measurements provide excellent temporal coverage of the 2006 event at a single point. To extend the spatial coverage, we use stacks of ascending and descending Envisat InSAR imagery. This combination of data is used (1) to demonstrate that the creep is localized on a narrow fault trace, (2) to measure the along-strike variations in fault creep, and (3) to invert for the depth extent of creep. The amount of moment released by aseismic creep can be used for seismic hazard assessment of the SHF and improving understanding of the relation between creep and earthquakes.

[6] The second goal is to document the slip history of the SHF over a longer time interval spanning 1992 to 2007 and compare these InSAR measurements with field measurements of the long-term creep record. A similar analysis has been performed by A. Van Zandt and R. Mellors (manuscript in preparation, 2009). In addition, the magnitude and
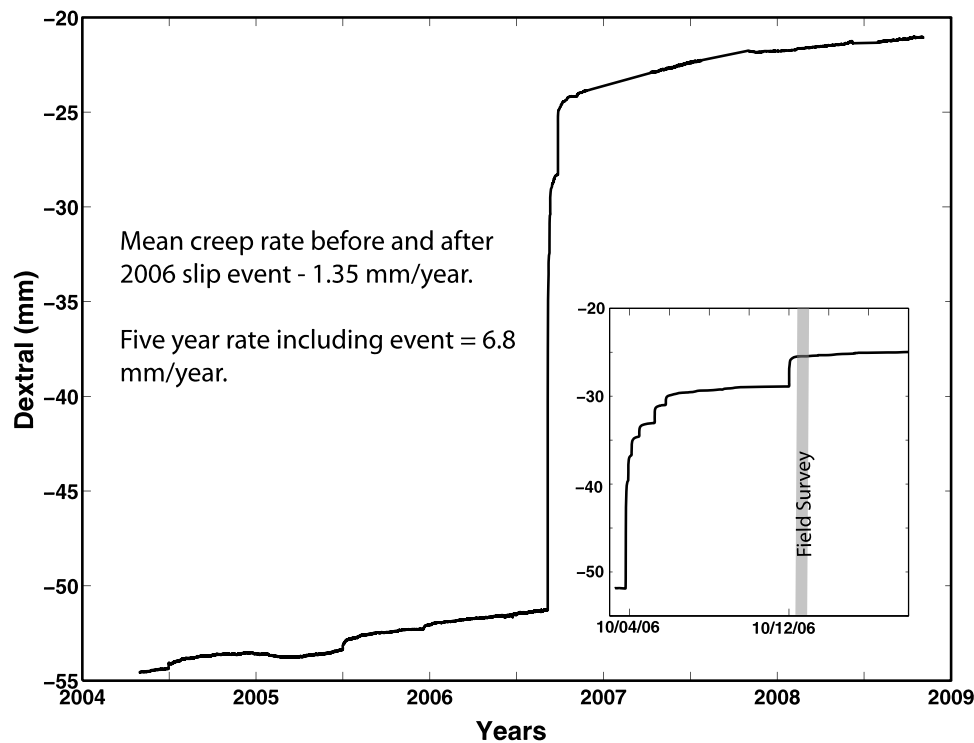
**Figure 2.** Creepmeter data from a new creepmeter installed by Roger Bilham beginning in 2004. It recorded 1.35 mm/a before and after the 2006 events during 2004–2009 (least squares fit). Compared to the ~27-mm creep event, the signal-to-noise level in the instrument is >1000:1. The inset in the right bottom corner is a zoom-in of slip during the 2006 events. The second field survey is on 12 October 2006, after the creep events ended. No slip was triggered on the Superstition Hills or San Andreas faults following a magnitude 4.5 earthquake on 3 November 2006, 41.7 km to the southwest of the creepmeter.

depth of the accumulated shallow creep is estimated and compared with the 2006 event.

[7] The third goal is to test the two-layer creep model for aseismic slip on the SHF proposed by *Bilham and Behr* [1992]. Creepmeter measurements following the Ms 6.6 1987 earthquake demonstrate that the time averaged slip rate decreases as a power law [*Bilham and Behr*, 1992]. The 3-year average creep rate between 1989 and 1991 was 28 mm/a while the average creep rate is about 6.8 mm/a between 2004 and 2006 based on creepmeter data. The creepmeter data show that long-term shallow creep consists of slow steady creep punctuated by accelerated creep events. Between 1989 and 1991 the creep rate during the events was about 10 times greater than the average creep rate between events. On the basis of this 10:1 ratio, *Bilham and Behr* [1992] proposed a two-layer model for aseismic slip on the SHF. During periods of the long-term shallow steady creep, the slip extends from the surface to a depth of about 300 m. During the creep events the slip extends 10 times deeper to a depth of about 3 km. The estimate of 3 km for the depth of the creep events was based on the abrupt increase in aftershock seismicity below approximately 3 km depth which also corresponds to the base of the sediments in the region [*Kohler and Fuis*, 1986]. Bilham and Behr speculated that the transition depth is sensitive to applied fault-normal stresses and suggest that the ratio of stable-sliding to episodic-slip velocities may provide an indication of secular variations in tectonic stress. Using

InSAR data we attempt to test the hypothesis that the depth of the long-term shallow steady creep is systematically smaller than the depth of the creep events. We find that the average shallow creep depth between 1992 and 2007 is similar to the depth of the 2006 event, both about 2–4 km. If this observation is correct then the slip is dominated by creep events from 1992 to 2007 and we cannot discriminate the depth of the shallow steady creep from the depth of the creep events using InSAR.

## 2. Data

[8] Following the observation of the SHF creep event starting on 6 October 2006 (R. Bilham, personal communication, 2006), we performed two field surveys: an initial reconnaissance survey on 8 October and a second more detailed survey in collaboration with Rob Mellors and Afton Van Zandt from San Diego State University on 12 October 2006. Because small surface cracks associated with creep can be degraded quickly by wind and especially rain, it was important to make measurements soon after the event [*Rymer et al.*, 2002]. Fortunately, the cracks were visible on the surface for more than 3 months following the event due to the lack of rain. In this region, the surface is arid and the creep amplitude was substantial (5–27 mm) making the surface cracks easy to trace for 8 km (Figure 3). The southernmost end of the rupture was located. But the northern end was not completely mapped because of time limitations. A typical surface offset is shown in Figure 3d.
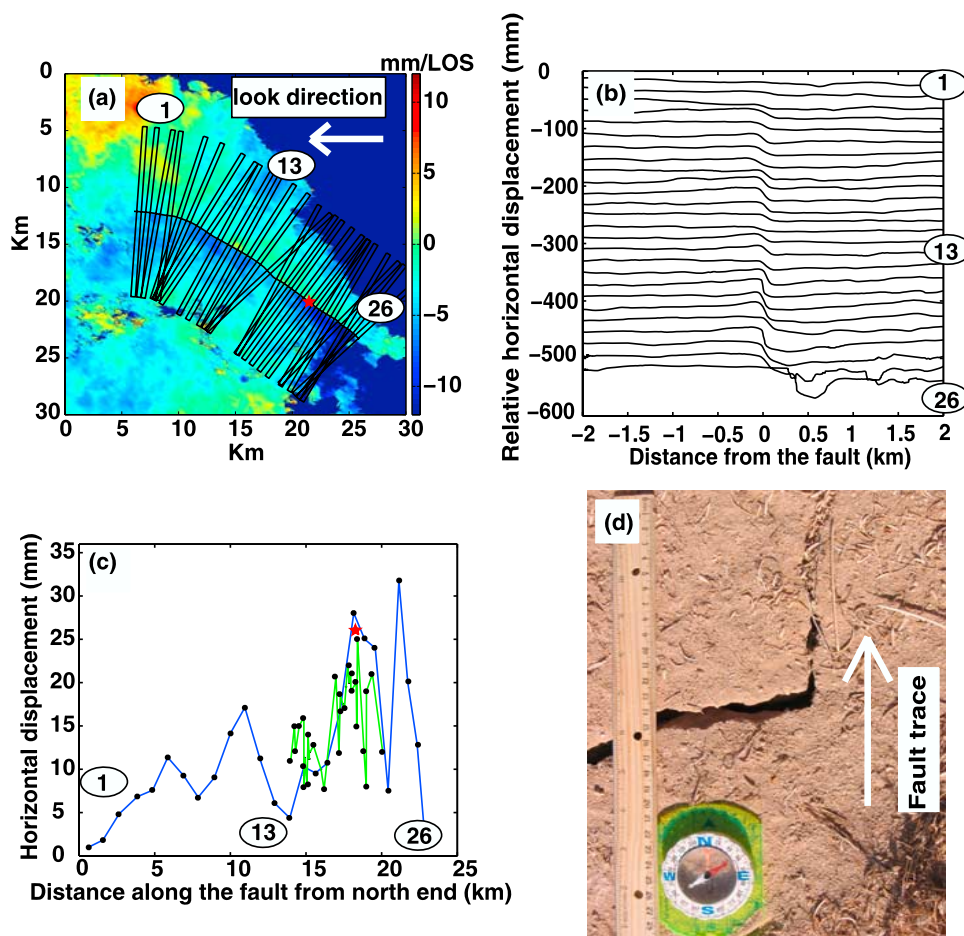
**Figure 3.** (a) Stack of seven descending Envisat interferograms spanning the 5 October 2006 creep event on the Superstition Hills segment of the San Jacinto fault zone. This event was measured/monitored on a creepmeter (red star) maintained by Roger Bilham, but this event was not detected by the sparse continuous GPS array or by nearby seismometers. (b) Line of sight (LOS) deformation along 26 profiles across the fault trace reveals a sharp step. (c) (blue) Peak-to-trough LOS deformation from interferometry compared with (green) field measurements made by students and faculty from University of California, San Diego, and San Diego State University just after the event and (red star) the creepmeter data. Black dots are data points. The LOS deformation from interferometry is projected to a horizontal displacement vector parallel to the fault strike, based on the assumption of no vertical slip. (d) The surface crack was measured over a length of 8 km, about one half of the total fault length. The lower amplitude of the field measurements with respect to the interferometry could indicate that some creep was underestimated in the field because it occurred off the main fault strand or rotation of en-echelon cracks occurred [*Bilham*, 2005].

Strike-slip displacement was measured along the trace of the rupture at approximately 100 m intervals. Extensional stepovers were identified and a ruler was placed over the crack and aligned in the direction of the overall fault trace (302° clockwise from north). Then the distance between conjugate piercing points was measured at two to three locations on each crack (Table 1). The averaged fault offsets are shown in Figure 3c.

[9] ERS-1/2 InSAR data covering a time period of more than 15 years constrain the long-term creep rate of the Superstition Hills fault, and 2 years of Envisat data constrain the displacement during the October 2006 event. Both ERS-1/2 and Envisat data along track 356 were collected by the European Space Agency and obtained through the Western North America Interferometric Synthetic Aperture Radar Consortium (WInSAR) archive (Figure 4). For the ERS-1/2 data, we processed two frames, 2925 and 2943, together to better estimate the long-wavelength error. Envisat data are used to image the 2006 creep event (ascending track 77, frame 657; descending track 356, frame 2943). The InSAR data was processed using SIOSAR software, and SRTM data were used to remove the topographic effect. Deformation along the southernmost end of the SHF was not fully recovered because all interferograms were decorrelated in the agricultural areas of the Imperial Valley.

[10] A combination of sparse GPS and dense InSAR is used to recover the surface deformation over the length scales needed to estimate slip versus depth. The field measurements only provide the slip on the trace of the

**Table 1.** Field Measurements of Fault Offset Collected on October 12, 2006, Along the Superstition Hills Fault

| Longitude | Latitude | Displacement[a] (mm) |
|---|---|---|
| −115.73436 | 32.95717 | 11 |
| −115.73231 | 32.95489 | 15 |
| −115.73175 | 32.95372 | 12 |
| −115.72964 | 32.95194 | 15 |
| −115.72703 | 32.95025 | 16 |
| −115.72701 | 32.95017 | 8, 11, 9 |
| −115.72650 | 32.94987 | 10, 12, 12 |
| −115.72689 | 32.94908 | 8 |
| −115.72527 | 32.94903 | 8, 9, 8 |
| −115.72467 | 32.94869 | 14 |
| −115.72397 | 32.94828 | 12 |
| −115.72400 | 32.94826 | 12, 11, 12, 10, 11 |
| −115.72364 | 32.94798 | 13, 12, 11 |
| −115.72161 | 32.94650 | 12, 13, 13 |
| −115.71745 | 32.94338 | 9, 11, 10 |
| −115.71571 | 32.94203 | 6, 8, 9 |
| −115.70904 | 32.93674 | 21, 21, 20 |
| −115.70737 | 32.93535 | 12, 12, 12 |
| −115.70659 | 32.93469 | 15, 19, 20, 20 |
| −115.70517 | 32.93358 | 16, 19 |
| −115.70430 | 32.93297 | 16, 19, 16 |
| −115.70341 | 32.93216 | 18, 21 |
| −115.70248 | 32.93146 | 22 |
| −115.70164 | 32.93082 | 21, 19 |
| −115.70078 | 32.93014 | 21 |
| −115.70066 | 32.93002 | 20, 22, 15 |
| −115.69772 | 32.92747 | 20 |
| −115.69739 | 32.92716 | 15 |
| −115.69700 | 32.92686 | 25 |
| −115.69331 | 32.92375 | 12 |
| −115.69206 | 32.92282 | 8 |
| −115.69194 | 32.92258 | 19 |
| −115.68862 | 32.92032 | 21 |
| −115.68287 | 32.91647 | 12 |

[a]There are three groups of surveyors, and the record format is not exactly same. For example, only the central group measures each location three times.

fault. Estimation of the slip from the surface to the base of the seismogenic zone (10–14 km) requires deformation measurements extending between 0 and 14 km from the fault. This wide range of length scales requires both minimal smoothing of the interferograms as well as incorporating long-wavelength constraints from the GPS-derived SCEC V3.0 velocity model [*Shen et al.*, 1996]. We use a remove/restore method to combine the GPS and InSAR along with stacking to minimize the InSAR errors [*Lyons and Sandwell*, 2003]. Deviations from the standard InSAR processing consisted in the following steps: (1) compute the line of sight (LOS) model phase difference from the SCEC velocity model and map into radar coordinates using a topographic phase mapping function; (2) compute the amplitude dispersion [*Ferretti et al.*, 2001] of all aligned SAR images to use as a weight function for the spatial filtering of the interferograms; (3) low-pass filter each single-look interferogram using a Gaussian filter with a 0.5 gain at a wavelength of 100 m; (4) stack the residual phase of the interferograms and remove a planar surface from the stack; and (5) restore the LOS phase from the SCEC velocity model.

## 3. Displacement Along the Fault

[11] To begin the analysis we compared the fault slip measured in the descending stacked interferogram cover-

ing a time period of 2 years (Figure 3a) with the offsets measured in the field. The LOS displacement is measured by taking the difference of maximum and minimum value within 1 km from the fault after the profile is flattened. In this way, the LOS displacement will not be underestimated even though the interferograms are smoothed by the Gaussian filter. Atmospheric errors should be less than 3 mm, considering the fact that seven images are stacked and the horizontal length scale is small [*Emardson et al.*, 2003]. In order to compare the InSAR measurements with the field measurements, pure strike slip is assumed (as confirmed by data from the ascending orbit and three-dimensional modeling discussed below), and LOS measurements are converted to strike-slip displacement based on satellite and fault geometry. The fault azimuth is 302° clockwise from north and the local incidence angle of the satellite is 23°. We use a local incidence angle for the finite fault inversion and a constant 23° incidence angle for the antiplane dislocation model.

[12] Results from the creepmeter, InSAR, and field measurements are compared in Figure 3c. All three measurements are consistent at the location of the creepmeter where the displacement is 27 mm. In general there is good agreement between the field measurements and the InSAR data, which confirm that the creep has a negligible (if any) dip-slip component and is confined to a very narrow zone. The InSAR step appears smooth (∼50 m) because of the low-pass Gaussian filter that was applied to reduce the phase noise. The dextral horizontal displacement along SHF shows two lobes with a minimum at the along-fault distance of ∼13 km (Figure 3c). The along-fault variations in displacement for the 2006 event are very similar to the field measurements of fault creep made in 1999 just after the Hector Mine earthquake, and the fault offset for both the 2006 and 1999 creep events is similar in magnitude to events in 1968, 1979, and 1987 as compiled by *Rymer et al.* [2002].

[13] In addition, we estimate the along-strike slip variation from 1992 to 2007 using both individual and stacked interferograms. The slip that accumulated between 1992 and 2007 is compared with the slip measured by *Rymer et al.* [2002] for the slip events (Figure 5). The InSAR result is consistent with field measurement for slip events in 1999 and 2006, which lends support to the validity of the method. Many of the slip inferred from the InSAR measurements for the 1999 event are significantly larger than the slip reported from the field measurements, probably because the deformation zone is wider than the cracks seen in the field, or additional displacement occurred shortly after the field measurements. The slip during 1993–1996 is substantial, with a maximum slip rate of 10 mm/a, which exceeds the steady background slip rate between 1989 and 1992 [*Bilham and Behr*, 1992] derived from creepmeter data. We hypothesize that one or more creep events occurred between 1993 and 1996. Similarly the average slip between 1992 and 2007 is higher than the background slip rate and the slip is relatively uniform along the fault; both observations suggest slip occurred in multiple events and the stable creep and episodic creep events have a different spatial distribution along the fault. Next, we examine slip varia-
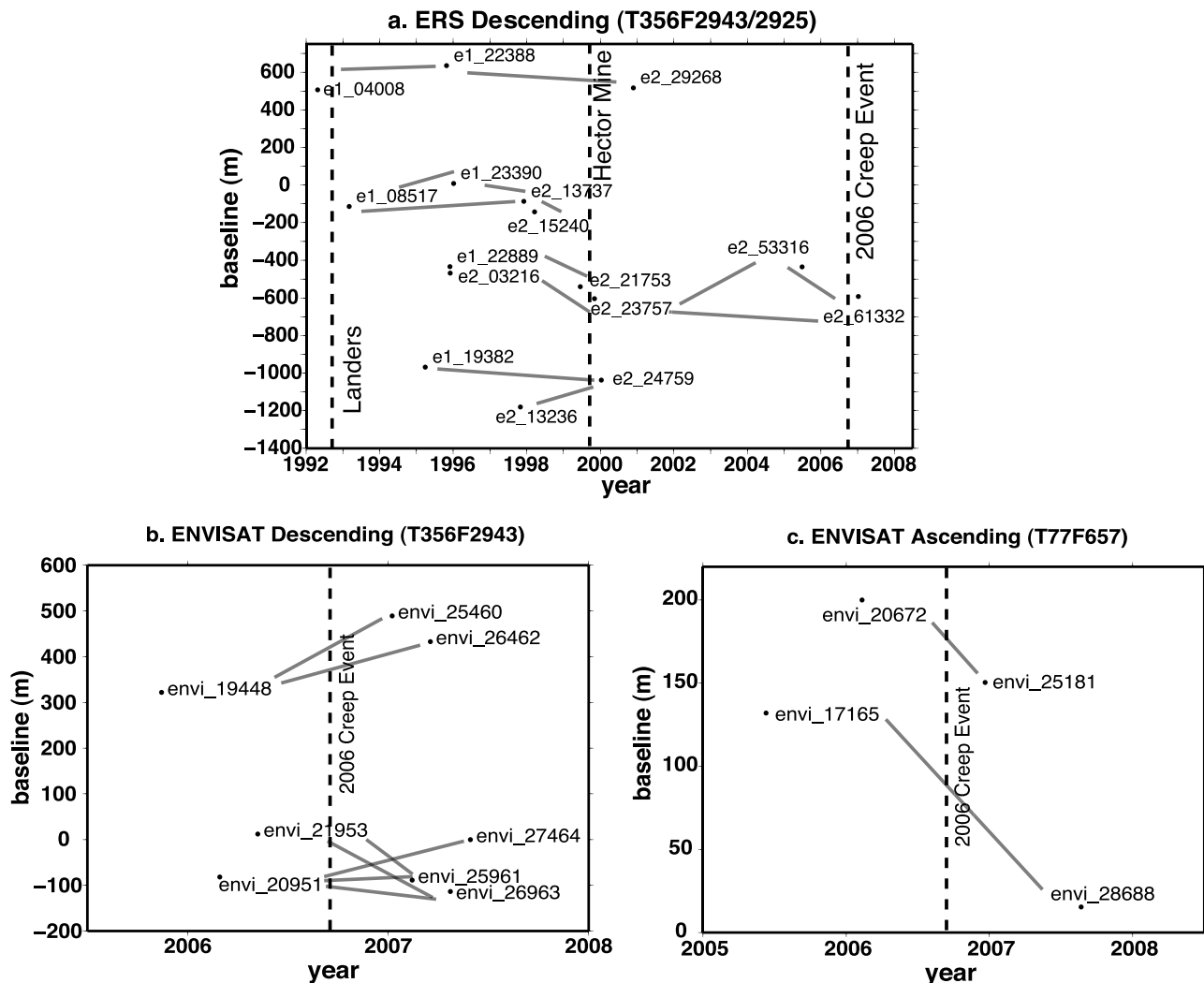
**Figure 4.** Interferometric synthetic aperture radar (InSAR) data used in this research. (a) ERS-1/2 descending data for the long-term slip (track 356, frame 2943/2925). The dashed lines label the times of the Landers and Hector Mine earthquakes and the 2006 creep event. (b) Envisat descending data (track 356, frame 2943) for the 2006 creep event. (c) Envisat ascending data (track 77, frame 657) for the 2006 creep event. The dashed lines in Figures 4b and 4c indicate the time of the 2006 creep event.

tions with distance from the fault to estimate the slip distribution with depth.

## 4. Estimates of Slip Versus Depth Using a Finite Fault Model

[14] Solutions for surface displacements due to dislocations in an elastic half-space are readily available for both homogeneous [*Okada*, 1985] and layered media [*Wang et al.*, 2003]. To model the displacement for the 2006 creep event, we use the finite fault homogeneous Greens function [*Okada*, 1985]. This finite fault model is appropriate for a short-term event because, as we demonstrate below, most of the slip occurred in the shallow crust. However, to model the long-term slip from 1992 to 2007, we need to account for the fault slip below the brittle-ductile transition. Expecting less variation of slip along the fault during the interseismic period and trying to simplify the modeling of the interseismic slip, we use the Green's function for an anti-

plane dislocation model for the long-term slip [*Savage et al.*, 1981]. Although the Superstition Hills fault cuts through thick sediments through overlying bedrock [*Kohler and Fuis*, 1986], the principal effect of increases in rock rigidity with depth is a small shift in the inferred slip distribution toward shallower depth [*Cohen*, 1999; *Fialko*, 2004]. So we ignore the effects of layering in our analysis. In order to do a direct comparison of the slip depth between the 2006 creep event and the long-term slip, we model the 2006 creep event using the antiplane dislocation model as well.

[15] Slip inversions using coseismic and postseismic deformation data are well established techniques [*Nielsen et al.*, 1995; *Murray and Segall*, 2002; *Fialko et al.*, 2005]. A homogeneous half-space elastic model is used to estimate the strike-slip and dip-slip components at depth by least squares fitting the surface deformation data (Figures 6–8). The detailed procedure and data reduction method can be found in the work of *Fialko* [2004]. To stabilize the inversions in the presence of long-wavelength noise (mainly
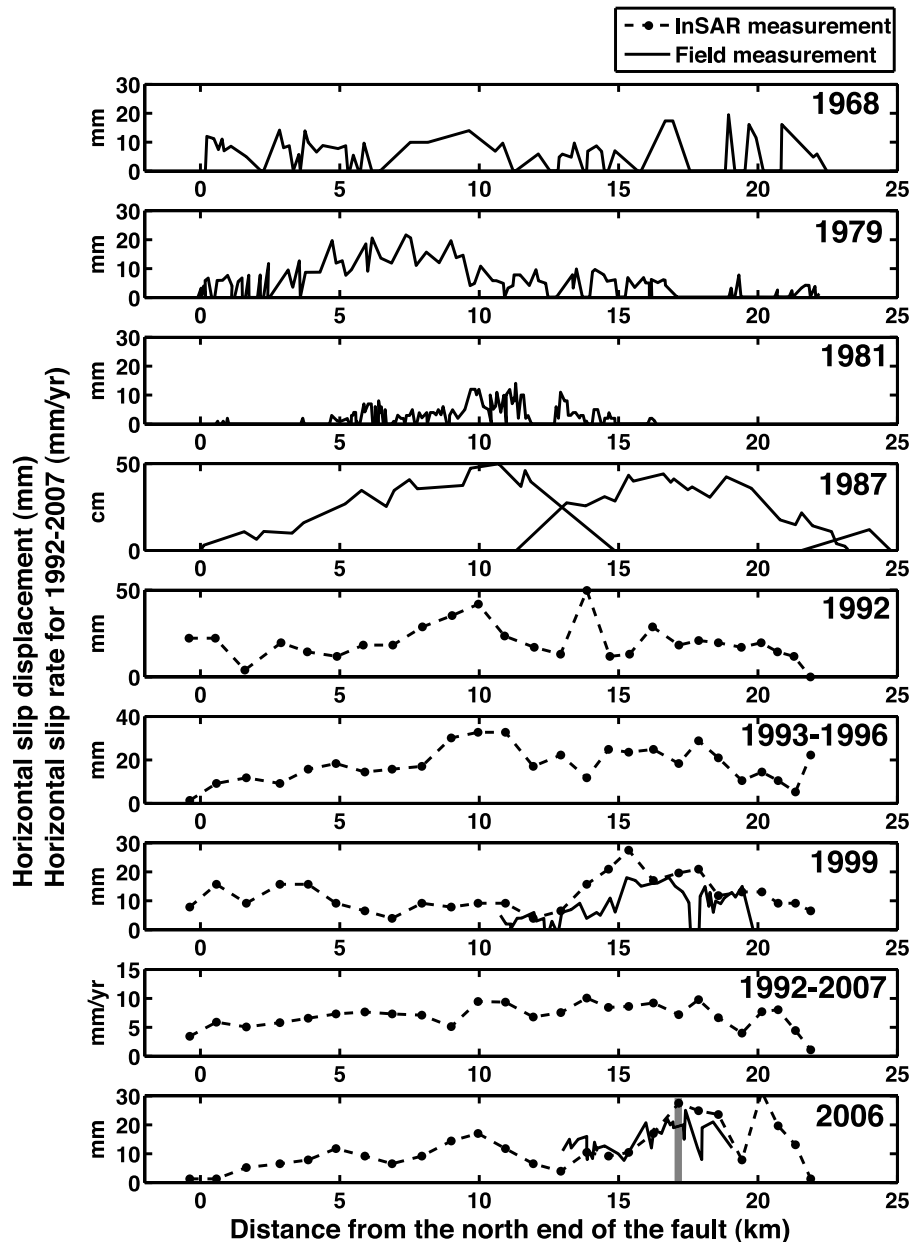
**Figure 5.** Slip distribution along the SHF during seven slip events. The $y$ axis is displacement, except for 1992–2007, for which it is slip rate. Solid lines are field measurements, while dashed lines are InSAR measurements. Field measurements of 1968, 1979, 1981, 1987, and 1999 are digitized from *Rymer et al.* [2002]. No field measurements were made on the northern part of the fault (0–10 km) for the triggered event in 1999. Field measurement of the 2006 event and all InSAR measurements are from this study. There are no short-duration interferometric pairs spanning the 1992 Landers earthquake, so a residual interferogram is generated by subtracting e1_08517_e1_23390 from e1_04008_e1_223881009. Black dots are the data sampling of InSAR measurements. The 1987 displacement is measured 12 days after the earthquake. The vertical shaded bar for the 2006 event shows the location of the Caltech/University of Colorado creepmeter. The 0 km is at N32.023 W115.853.

atmospheric noise), we perform an irregular spatial sampling of the data based on the distance from the fault (Figure 7). Since the displacement signal is near-field and low amplitude, it is crucial to describe the surface trace of the fault as accurately as possible. We use 26 segments, based on the U.S. Geological Survey (USGS) regional fault map and B4 Laser altimetry data [*Bevis et al.*, 2005] to model the 20-km-long SHF. Since the inversions are inherently nonunique, additional constraints are added to regularize the inversion. We prohibited sinistral slip by using a Coleman algorithm, which is the default in MATLAB function "lsqlin" [*Coleman and Li*, 1996]. Wild spatial variations in slip were suppressed by using a Laplacian smoothness constraint. The smoothness weighting parame-
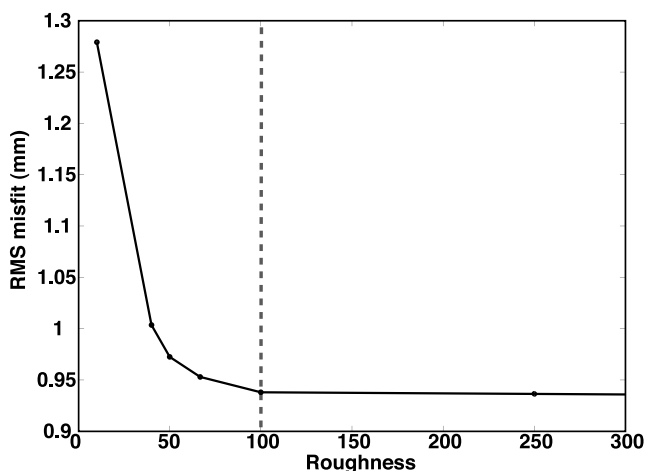
**Figure 6.** LOS RMS misfit versus roughness for the finite fault model inversion. The black dots are the sampling data. The dashed line indicates the value we use for roughness, 100.

ter controls the smoothness of the slip model. The RMS misfit of the model is inversely related to the smoothness weighting parameter, which is a classic trade-off, as shown in Figure 6. We use this trade-off to seek the "smoothest" slip distribution with the lowest RMS misfit. RMS misfit is defined as $\chi = \sqrt{\left(\sum_{i=1}^{N}(d_i - d_i^m)^2\right)/N}$, where $d_i$ is the LOS displacement on sampled InSAR data points (both ascending and descending), $d_i^m$ is the modeled LOS displacement on the sampled points, and $N$ is the total number of the sampled points.

[16] The data and modeled interferograms are illustrated in Figure 7 for both descending and ascending LOS directions. The misfit is 1.0 mm LOS for ascending data and 0.9 mm LOS for descending data. The relatively large anomaly at the very southern end of the fault in the descending residual might be due to creep on a subfault in the irrigation area. Because it is only an edge effect for our inversion and no useful ascending data cover that subfault, we did not include it in our model. The slip versus depth distribution shown in Figure 8 indicates that most slip is confined to depths less than 3 km and maximum slip occurs at the surface. The model has only a small component of vertical fault slip (<10%), which validates our assumption of pure horizontal slip. There are two patches of high slip along the fault. The north segment slips less than the south segment, with an average dextral slip of about 9 mm and 13 mm respectively, which is consistent with the fault offset observed in the field (Figure 3). Using a "nominal" value of the shear modulus of 33 GPa [*Becker et al.*, 2005], the moment of this slip event is $1.3 \times 10^{23}$ dyn cm. This corresponds to a moment magnitude of $M_W$ 4.7 earthquake [*Kanamori*, 1977]. Since the fault slipped slowly over a period of 9 days, no seismic waves were generated. No aftershocks were detected by the regional seismic arrays or local portable seismometers.

## 5. Antiplane Dislocation Model for Both the Creep Event and the Long-Term Slip

[17] Modeling the long-term slip requires consideration of the entire depth range from the surface to well below the brittle-ductile transition. The deep slip is most easily parameterized by an antiplane dislocation extending from the
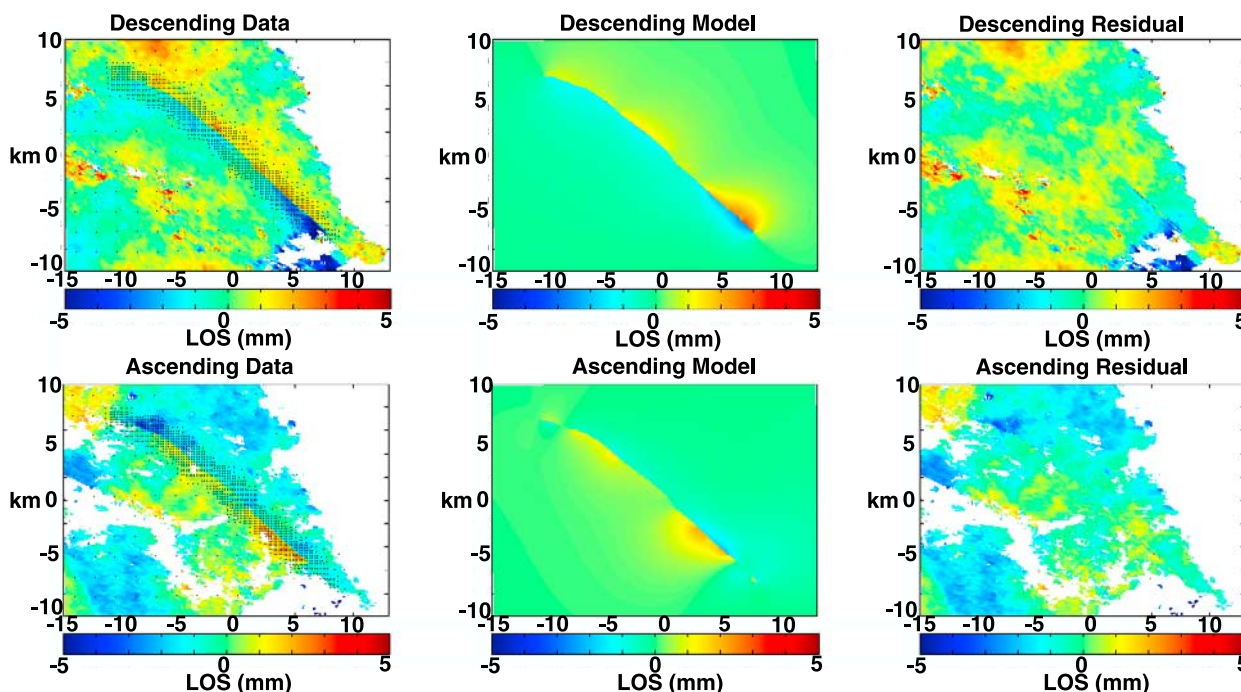


**Figure 7.** (left) InSAR data, (middle) the best fitting model, and (right) the residual for the 2006 event. The black dots in InSAR data figures are subsample locations of data that are used in the inversion.
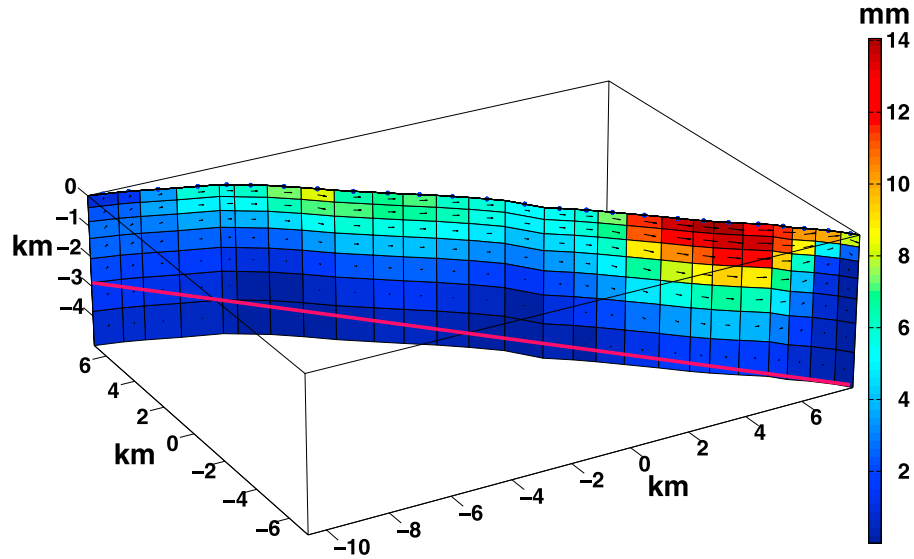
**Figure 8.** The slip distribution for the 2006 creep event using a finite fault model. The patch size along the fault varies from 0.5 km to 0.9 km. The patch size in depth varies from 0.4 km to 1 km, increasing with depth. The arrow shows the relative size and direction of vertical and horizontal slip. The pink link is the sediment depth from seismic reflection data [*Kohler and Fuis*, 1986].

locking depth to infinity. To compare the 2006 creep event to the long-term slip we repeat the event analysis of section 4 using an antiplane dislocation model. A discrete slip model has been used to compute the surface profile. However, the shallow locking depth estimated from the discrete slip model is not realistic and should not be regarded as the true locking depth [*Savage*, 2006]. Therefore we use a model assuming piecewise constant variations in fault slip with depth based on the antiplane dislocation model that consists of a dextral strike-slip dislocation in an elastic half-space [*Weertman*, 1965; *Cohen*, 1999]. The surface displacement $v(x)$ is given by

$$v(x) = \int_{-\infty}^{0} \frac{x}{x^2 + z^2} m(z) dz, \tag{1}$$

where $x$ is the distance from the fault trace, $z$ is the depth and $m(z)$ is the slip distribution versus depth.

[18] The model is parameterized in layers with uniform slip in each layer. In this case, the slip distribution $m(z)$ in equation (1) can be set up as a linear programming problem with a smoothness constraint in the form of Laplacian operator $\nabla^2$,

$$\min ||(Am - b)/\sigma||^2 + \lambda||\nabla^2 m||$$
$$\text{subject to } m > 0, \tag{2}$$

where $b$ is the observed surface displacement as a function of distance from the fault trace, $\sigma$ is the uncertainty in the observation, $m$ is fault slip versus depth, $\lambda$ is the weighting

factor of smoothness, and $A$ is a matrix of the Green's function,

$$
\begin{aligned}
A_{ij} &= \int_{z_j}^{z_{j-1}} \frac{x_i}{x_i^2 + z^2} dz \\
&= \int_{z_{j-1}}^{0} \frac{x_i}{x_i^2 + z^2} dz - \int_{z_j}^{0} \frac{x_i}{x_i^2 + z^2} dz \\
&= \tan^{-1} \frac{x_i}{z_j} - \tan^{-1} \frac{x_i}{z_{j-1}},
\end{aligned} \tag{3}
$$

where $x_i$ is the distance from the fault, $z_j$ is the depth of the top of a layer and $z_{j-1}$ is the depth of the bottom of a layer.

[19] The inversion is more sensitive to the shallow slip than to the deep slip so the layer thickness was adjusted to increase with depth from 200 m to 1800 m. The last layer extends from the maximum depth of seismicity in the region (14 km) to infinity. As a consequence, the entry in the matrix $A$ that corresponds to the last layer is calculated with a single arctangent function. The 100-m wavelength spatial Gaussian filter that was applied to the interferogram was also applied to the Greens functions in the matrix A to make the model smoothness match the data smoothness.

[20] Sixteen fault-perpendicular profiles were extracted from interferograms in rectangular boxes 400 m wide and up to 40 km long. Data near the ends of the fault were not used to avoid the 3-D edge effects. Profiles were binned at an even 100 m spacing away from the fault [*Parker*, 1977; *Parker and Song*, 2005]. The smoothness parameter was selected as a trade-off between model smoothness and RMS misfit. Because the east side of the SHF is close to farm land, where InSAR data are decorrelated, there is only 5 km of data on the east side of each profile, while data to the west of the fault provides much better coverage (>30 km).
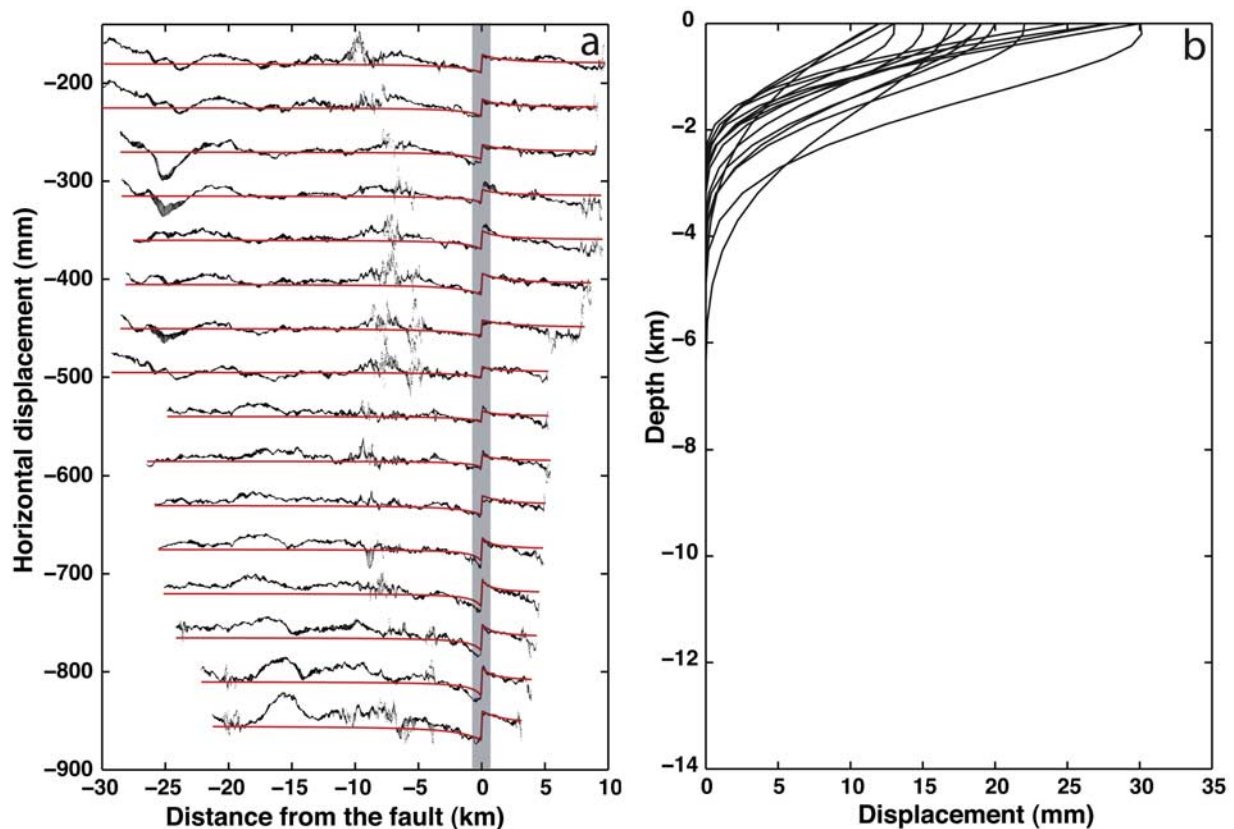
**Figure 9.** Profiles of the 2006 slip event on the SHF and the best fitting antiplane dislocation models. (a) Profiles and best fitting antiplane dislocations. The black lines are the InSAR data with boxes 400 m wide and 40 km long, and the red lines are the best fitting models. The $y$ axis is the relative slip displacement. (b) Slip in depth distribution of the best fitting models for the creep event. Smoothness constraint is chosen from the trade-off between misfit and smoothness. The result shows that the creeping depth is about $2-4$ km for the event. The sharp signal at 10 km left of the fault (Figure 9a) is not aligned with Superstition Hills Mountain fault.

The model successfully reproduced the surface deformation for all 16 profiles, and the average root mean square (RMS) misfit is 6 mm (Figure 9). The sharp step near the fault is caused by the shallow slip. The magnitude of the slip varies along the fault (as seen from variations between different profiles). However, the decay pattern with depth is similar for all profiles. The far-field deformation vanishes away from the fault, suggesting there is no deep slip for the 2006 creep event. In all cases, the slip has a maximum at the surface and then decays rapidly to zero slip at $2-4$ km depth. Many of the profiles show a high noise area about 1 km to the west of the fault. This is likely to be a consequence of stacking several interferograms with similar atmospheric error and less than optimal correlation. To the north of the SHF (Figure 1), a large range change in LOS is observed and is likely explained by ground subsidence due to the groundwater extraction [*Mellors and Boisvert*, 2003].

[21] The same antiplane dislocation inversions were performed on 16 profiles extracted from the long-term stack (1992–2007). These profiles generally have a lower noise level because more data are available for stacking. The antiplane dislocation model also shows a good fit to all the profiles with an average RMS misfit of 1.1 mm/a (Figure 10). The slip versus depth models show shallow and deep slipping zones separated by a locked zone from 3 to 7 km deep. The shallow slip has a peak at the surface and decays rapidly to zero at $2-4$ km depth. This is very similar to the slip versus depth distribution derived from the interferograms spanning the 2006 event. In addition, the long-term models all have a deep-slip component that matches the nearly linear trend in the data profiles far from the fault. As discussed above, this trend is constrained by the SCEC velocity model, which is based on GPS measurements. We find there is a trade-off between the locking depth and the deep slip rate. On the basis of the maximum depth of the aftershocks following the 1987 earthquake, we chose the upper edge of the deepest layer to be 14 km [*Lin et al.*, 2007]. In the inversion, a deep slip rate of about 30 mm/a from 1992 to 2007 is preferred. However, as discussed below, an unknown fraction of the linear trend could be due to interseismic slip on nearby faults such as the San Andreas/Brawley seismic zone, Superstition Mountain, or Imperial faults. Therefore, we cannot constrain the deep slip rate using the InSAR data.

[22] To estimate how deep slip from nearby faults might contribute to our inversion (without constructing a comprehensive interseismic model across the plate boundary), we reran the inversion on a representative profile (number 11)
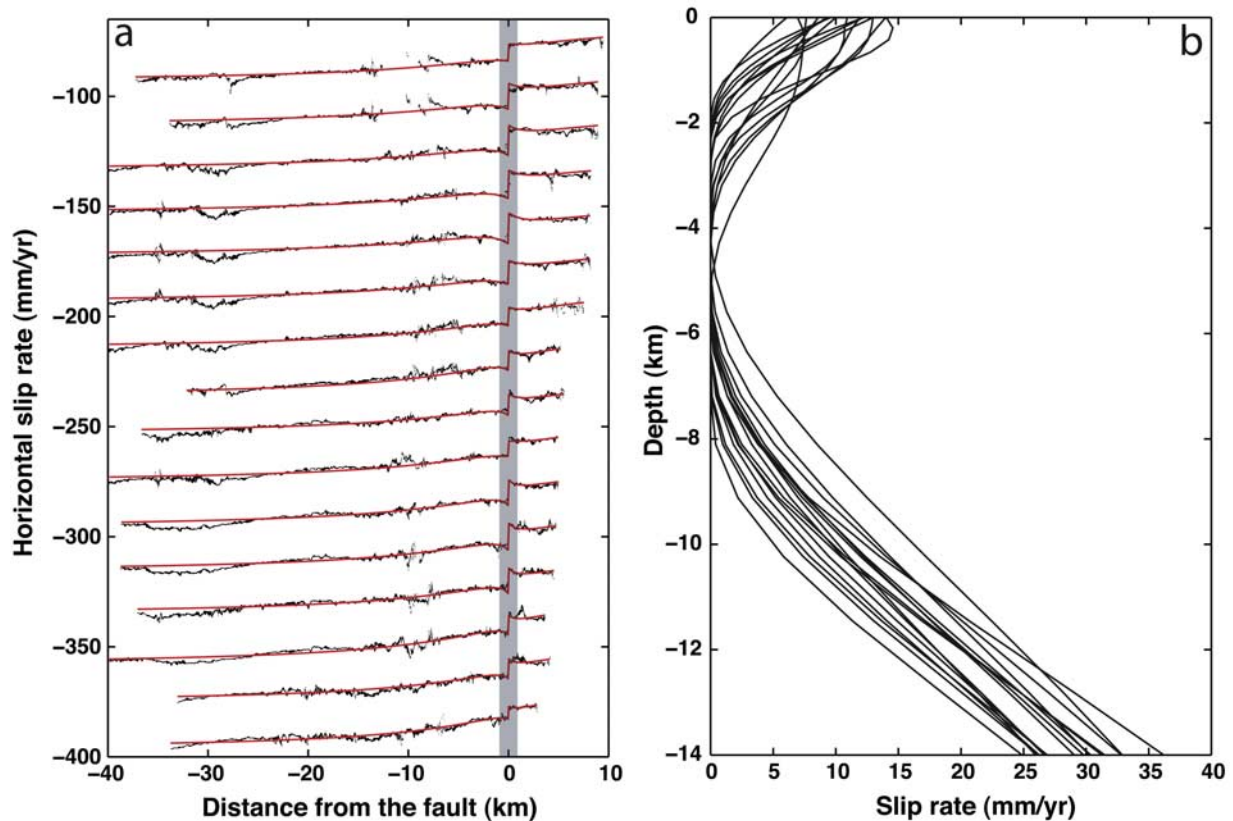
**Figure 10.** Profiles of the 1992–2007 interferograms on the SHF and the best fitting models. (a) Displacement profiles across the fault and the predicted slip displacement from the model. The black lines are the InSAR data with boxes 400 m wide and 40 km long, and the red lines are the best fitting model. The $y$ axis is the relative slip rate. (b) Slip in depth distribution of the best fitting models for the slip during 1992–2007. Smoothness constraint is chosen from the trade-off between misfit and smoothness. The result shows that the shallow creeping depth is about 2–4 km. The slip in depth distribution pattern looks like a mirror image of the seismic moment distribution found for several large earthquakes around the world [*Fialko et al.*, 2005].

and removed a linear trend from the data. As a consequence, the deep slip rate decreases as the linear trend is removed. When a linear trend of 0.2–0.3 mm/a/km is removed, the deep slip rate is consistent with independent estimates for long-term slip rate on this fault, which ranges from 1.7 to 5.5 mm/a, based on paleoseismic evidence [*Hudnut and Sieh*, 1989]. Despite the amount of linear trend that is removed all the inversions show similar patterns of shallow slip between 0 and 4 km deep (Figure 11); there is a maximum in slip rate at the surface that decreases to zero slip at 4 km depth, which is required to fit the sharp curvature in the horizontal displacement between 0 and 4 km from the fault on both sides. At depths greater than 5 km the estimates of slip rate are highly dependent on the removed linear trend. High linear trend removed (>0.2 mm/a/km) result in no slip in the seismogenic layer (at depths between 4 and 9 km). In contrast, low linear trend removed (<0.2 mm/a/km) result in low slip rate between 4 and 9 km. Understanding the slip rate at greater depths will require a more complete regional analysis that includes a three-dimensional finite fault interseismic model of all

major faults of the southern San Andreas system and the cross-faults which parallel to the Elmore Ranch fault.

## 6. Discussion

[23] Previously published data from creepmeter measurements have demonstrated that creep on the SHF consists of a secular background creep and a decaying postseismic transient that are punctuated by episodic creep events [*Bilham and Behr*, 1992]. The quasisteady creep was highest just after the 1987 earthquake (28 mm/a) and slowed to 2.4 mm/a between May 1989 and July 1991. Creepmeter data were unavailable from 1992 to 2004. One question is whether the postseismic transient still affects the present-day deformation. We divided the average slip along the SHF fault for each interferogram by the time interval of the interferogram (Figure 12). To make sure that the result represents average slip, we excluded interferograms with a time interval shorter than 2 years. Usually one needs to stack several interferograms to reduce the atmospheric error. However, for our purpose, atmospheric error is negligible because the creep signal is localized within 1 km of the fault
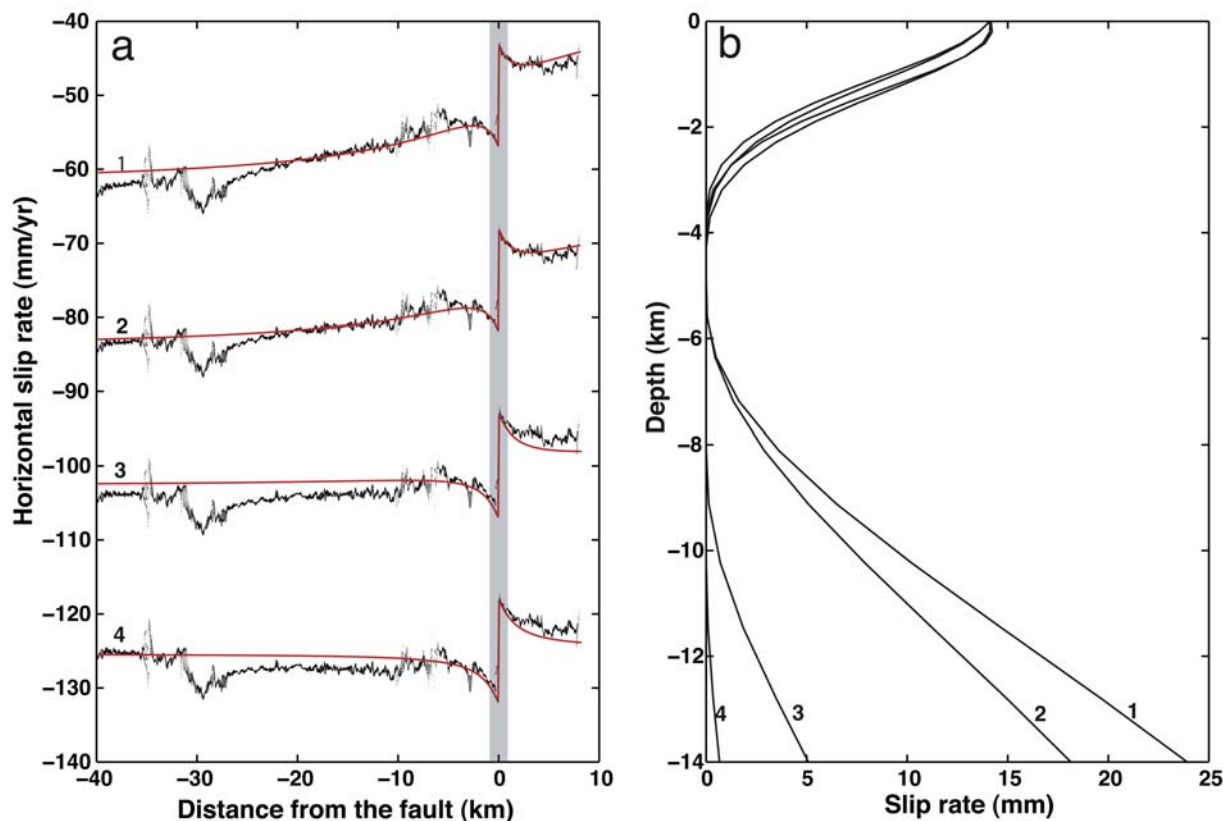
**Figure 11.** The effect of interseismic deformation on nearby faults on slip inversion. (a) InSAR profile 11 (see Figure 3a) and best fitting models for data with different linear trends removed: (1) no trend removed, 24 mm/a deep slip rate; (2) 0.1 mm/a/km, 17 mm/a deep slip rate; (3) 0.2 mm/a/km, 5 mm/a deep slip rate; and (4) 0.3 mm/a/km, 0.5 mm/a deep slip rate. The black lines are InSAR data with different trends removed and red lines are the best fitting models. (b) Slip rate distribution along depth for the best fitting models (1–4). The high curvature near 4 km on both sides of the fault is a robust indication of a locked zone in the middle of the crust.

and changes in the atmospheric contribution are typically not large over this length scale. In the context of afterslip after the 1987 SHF earthquake, we compare our data with two afterslip models, both stemming from the rate and state friction formulation but in different ways. The first model (Figure 12, solid curve), a prediction of the rate-and-state theory [*Dieterich*, 1979; *Marone et al.*, 1991], is $S(t) = b[1/(1 + t/(a/b))]$, where $S(t)$ is the slip rate, $t$ is time after the earthquake, $a$ and $b$ are rate-and-state parameters estimated from creepmeter data on the SHF between 1987 and 1992 ($a = 53.45$ and $b = 302.2$ in Figure 12) [*Marone et al.*, 1991; *Wennerberg and Sharp*, 1997]. The second model (Figure 12, dashed curve), a prediction from the generalized rate-and-state model [*Rice et al.*, 2001; *Barbot et al.*, 2009], is $S(t) = A(\coth(k/2)e^{kt/t_0}/(1 - [\coth(k/2)e^{kt/t_0}]^2)) + c$, where $A, k, t_0$ and $c$ are empirical constants ($A = -20, k = 5, t_0 = 25$ and and $c = 0.5$ in Figure 12). Both models describe afterslip on a fault plane driven by coseismic stress changes and have decaying velocity with time but have different asymptotic behavior; the first model does not have a well-defined limit of full relaxation, while the second model eventually returns to the background (interseismic) slip rate. The similarity between the two models during the early relaxation epoch as well as the large uncertainty in the InSAR data does not

allow us to discriminate between them. Also we cannot conclude that the slip rate is decaying during 1992–2008 time interval. However, in the 11 years prior to the 1987 earthquake, the shallow creep rate was only 0.5 mm/a [*Louie et al.*, 1985] which is much lower than any of the post earthquake measurements. This suggests that the postseismic transient from the 1987 earthquake might be still occurring.

[24] *Sieh and Williams* [1990] estimated the depth (0.6–2.7 km) of shallow creep and compared it with the sediment depth (1.3–3 km) of the Coachella Valley segment of the San Andreas Fault. They concluded that the high pore pressures in the sediments could produce a weak zone by reducing the effective normal stress in the upper 1 or 2 km of the fault, and the shallow creep is controlled by sediment depth, at least indirectly. Our study of the SHF is consistent with their conclusion. We find a maximum creep depth of 2–4 km where the sediment thickness varies between 3 km and 5 km [*Kohler and Fuis*, 1986].

[25] Our results from the interseismic modeling show both shallow and deep aseismic slip with a locked zone at depths between 4 and 6 km. This interseismic distribution of slip with depth is nearly a mirror image of the coseismic moment release versus depth inferred from several major
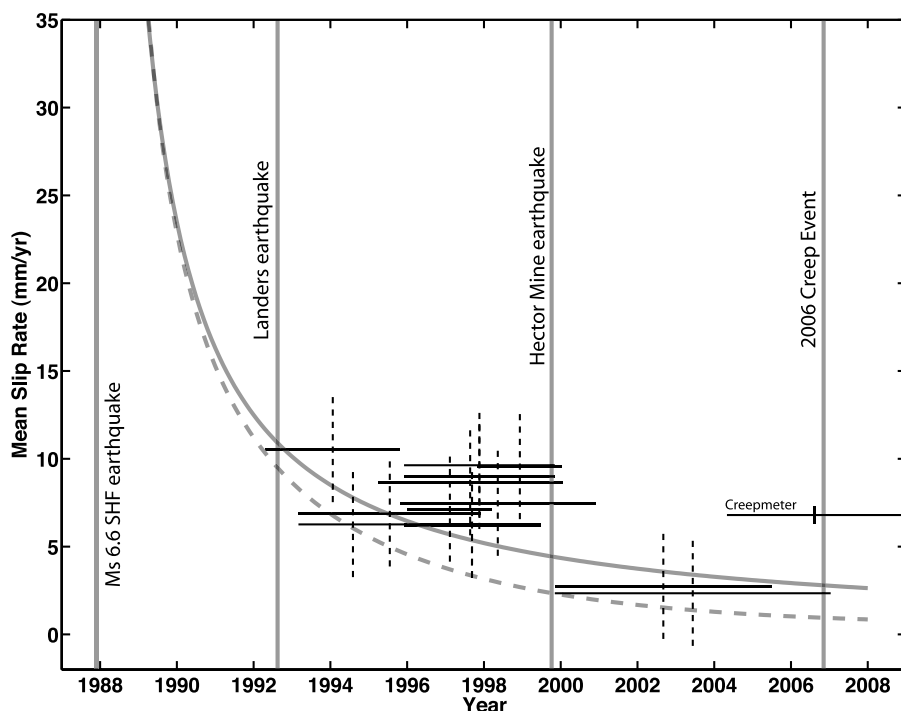
**Figure 12.** Slip history of the SHF from 1992 to 2008. The solid decay curve is the afterslip model based on the work of *Marone et al.* [1991, Table 3]. The dashed decay curve is a model based on *Barbot et al.* [2009]. All slip rates are taken from InSAR data with a time interval greater than 2 years, except the solid cross, which is from creepmeter data, 6.8 mm/a between March 2004 and October 2008. The range of the horizontal solid line is the time span of the interferogram or the creepmeter. The slip rate is calculated by dividing average displacement on the fault by the time span of the interferogram. The vertical dashed bar is the uncertainty of the slip rate (±3 mm/a, estimated from RMS of image). The uncertainty of the creepmeter data is set to 0.5 mm/a.

strike-slip earthquakes (Landers, $M_w$ 7.3, Hector Mine, $M_w$ 7.1, Izmit $M_w$ 7.6 and Bam $M_w$ 6.5) for which high-quality geodetic data are available [*Fialko et al.*, 2005]. All four earthquakes show shallow coseismic slip deficit. If the shallow coseismic slip deficit is a common feature of strike-slip faults, it must be compensated by postseismic afterslip, episodic slip events, continuous interseismic creep, or off-fault yielding [*Bodin et al.*, 1994; *Fialko et al.*, 2005]. The Superstition Hills fault displays all three types of localized shallow slip.

[26] We note that no seismic signal was detected by seismometers of the existing network during the 2006 creep event or by a seismometer installed on the fault after the creep event (E. Cochran, personal communication, 2007). The closest operating seismometer, SWS of the Caltech/USGS regional seismic network, was about 5 km away from the SHF trace (Southern California Earthquake Center). These observations suggest that the 2006 creep event was a spontaneous slip event that was neither triggered by, nor produced any seismic activity. This event was also not detected by the existing continuous GPS network. The closest available continuous GPS station, CRRS in the SOPAC network, is 9.3 km to the northeast. The precision of the GPS station is 1.1 mm in north, 1.3 mm in east, and 3.0 mm in up component, and the sampling rate is 1 Hz. On the basis of our finite fault slip model, the expected signal from the 2006 creep event is 0.9 mm north and 0.6 mm east. We checked the data in the CRRS station and found no

obvious signal around the time of the creep event. The lack of a resolvable signal at the closest GPS site is consistent with our inference that the creep occurred at a fairly shallow depth. It also illustrates difficulties associated with detection of shallow transient deformation using relatively sparse GPS arrays.

## 7. Conclusions

[27] The InSAR data, field measurements, and creepmeter data well document the surface deformation due to the 2006 creep event on the SHF (Figure 3). The maximum slip occurred along the southern end of the fault. The slip distribution along the fault is similar to the surface slip of the triggered event in 1999. Using InSAR, we detect at least three creep events. The creep event in 1992 is triggered by the Landers earthquake, the event in 1999 is triggered by the Hector Mine earthquake, and the 2006 event has no obvious triggering mechanism. The maximum shallow slip rate in the SHF is about 10 mm/a between 1992 and 2007, and the maximum surface displacement due to the 2006 event is about 27 mm. Both the 2006 creep event and the long-term slip, which includes several creep events, have maximum slip at the surface and decay to zero at depth of 2−4 km where the sediment thickness varies between 3 km and 5 km. Our results lend support to previous suggestions that the shallow creep is controlled by sediment depth, perhaps due to high pore pressures in the unconsolidated sediments.

## References

Allen, C. R., M. Wyss, J. N. Brune, A. Grantz, and R. Wallace (1972), Displacement on the Imperial, Superstition Hills, and San Andreas faults triggered by the Borrego Mountain earthquake, *U. S. Geol. Surv. Prof. Pap.*, *787*, 87–104.

Barbot, S., Y. Fialko, and Y. Bock (2009), Postseismic deformation due to the $M_w$ 6.02004 Parkfield earthquake: Stress-driven creep on a fault with spatially variable rate-and-state friction parameters, *J. Geophys. Res.*, doi:10.1029/2008JB005748, in press.

Becker, T. W., J. L. Hardebeck, and G. Anderson (2005), Constraints on fault slip rates of the southern California plate boundary from GPS velocity and stress inversions, *Geophys. J. Int.*, *160*, 634–650, doi:10.1111/j.1365-246X.2004.02528.x.

Bevis, M., et al. (2005), The B4 Project: Scanning the San Andreas and San Jacinto fault zones, *Eos Trans. AGU*, *86*(52), Fall Meeting Suppl., Abstract H34B-01.

Bilham, R. (1989), Surface slip subsequent to the 24 November 1987 Superstition Hills, California, earthquake monitored by digital creepmeters, *Bull. Seismol. Soc. Am.*, *79*, 424–450.

Bilham, R. (2005), Coseismic strain and the transition to surface afterslip recorded by creepmeters near the 2004 Parkfield epicenter, *Seismol. Res. Lett.*, *76*, 49–57, doi:10.1785/gssrl.76.1.49.

Bilham, R., and J. Behr (1992), A 2-layer model for aseismic slip on the Superstition Hills fault, California, *Bull. Seismol. Soc. Am.*, *82*, 1223–1235.

Bilham, R., N. Suszek, and S. Pinkney (2004), California creepmeters, *Seismol. Res. Lett.*, *75*, 481–492.

Boatwright, J., K. E. Budding, and R. V. Sharp (1989), Inverting measurements of surface slip on the Superstition Hills fault, *Bull. Seismol. Soc. Am.*, *79*, 411–423.

Bodin, P., R. Bilham, J. Behr, J. Gomberg, and K. W. Hudnut (1994), Slip triggered on southern California faults by the 1992 Joshua-Tree, Landers, and Big-Bear earthquakes, *Bull. Seismol. Soc. Am.*, *84*, 806–816.

Burford, R. O., and P. W. Harsh (1980), Slip on the San-Andreas-Fault in central California from alignment array surveys, *Bull. Seismol. Soc. Am.*, *70*, 1233–1261.

Burgmann, R., D. Schmidt, R. M. Nadeau, M. d'Alessio, E. Fielding, D. Manaker, T. V. McEvilly, and M. H. Murray (2000), Earthquake potential along the northern Hayward fault, California, *Science*, *289*, 1178–1182, doi:10.1126/science.289.5482.1178.

Cohen, S. C. (1999), Numerical models of crustal deformation in seismic zones, *Adv. Geophys.*, *41*, 133–231, doi:10.1016/S0065-2687(08)60027-8.

Coleman, T. F., and Y. Y. Li (1996), A reflective Newton method for minimizing a quadratic function subject to bounds on some of the variables, *SIAM J. Optim.*, *6*, 1040–1058, doi:10.1137/S1052623494240456.

Dieterich, J. H. (1979), Modeling of rock friction: 1. Experimental results and constitutive equations, *J. Geophys. Res.*, *84*, 2161–2168, doi:10.1029/JB084iB05p02161.

Emardson, T. R., M. Simons, and F. H. Webb (2003), Neutral atmospheric delay in interferometric synthetic aperture radar applications: Statistical description and mitigation, *J. Geophys. Res.*, *108*(B5), 2231, doi:10.1029/2002JB001781.

Ferretti, A., C. Prati, and F. Rocca (2001), Permanent scatterers in SAR interferometry, *IEEE Trans. Geosci. Remote Sens.*, *39*, 8–20, doi:10.1109/36.898661.

Fialko, Y. (2004), Probing the mechanical properties of seismically active crust with space geodesy: Study of the coseismic deformation due to the 1992 $M_w$ 7.3 Landers (southern California) earthquake, *J. Geophys. Res.*, *109*, B03307, doi:10.1029/2003JB002756.

Fialko, Y. (2006), Interseismic strain accumulation and the earthquake potential on the southern San Andreas Fault system, *Nature*, *441*, 968–971, doi:10.1038/nature04797.

Fialko, Y., M. Simons, and D. Agnew (2001), The complete (3-D) surface displacement field in the epicentral area of the 1999 $M_w$ 7.1 Hector Mine earthquake, California, from space geodetic observations, *Geophys. Res. Lett.*, *28*, 3063–3066, doi:10.1029/2001GL013174.

Fialko, Y., D. Sandwell, M. Simons, and P. Rosen (2005), Three-dimensional deformation caused by the Bam, Iran, earthquake and the origin of shallow slip deficit, *Nature*, *435*, 295–299, doi:10.1038/nature03425.

Funning, G. J., R. Burgmann, A. Ferretti, and F. Novali (2007), Creep on the Rodgers Creek fault, northern San Francisco Bay area from a 10 year PS-InSAR dataset, *Geophys. Res. Lett.*, *34*, L19306, doi:10.1029/2007GL030836.

Hudnut, K. W., and M. M. Clark (1989), New slip along parts of the 1968 Coyote Creek fault rupture, California, *Bull. Seismol. Soc. Am.*, *79*, 451–465.

Hudnut, K. W., and K. E. Sieh (1989), Behavior of the Superstition Hills fault during the past 330 years, *Bull. Seismol. Soc. Am.*, *79*, 304–329.

Hudnut, K. W., L. Seeber, and J. Pacheco (1989a), Cross-fault triggering in the November 1987 Superstition Hills earthquake sequence, southern California, *Geophys. Res. Lett.*, *16*, 199–202, doi:10.1029/GL016i002p00199.

Hudnut, K. W., L. Seeber, and T. Rockwell (1989b), Slip on the Elmore Ranch fault during the past 330 years and its relation to slip on the Superstition Hills fault, *Bull. Seismol. Soc. Am.*, *79*, 330–341.

Kanamori, H. (1977), The energy release in great earthquakes, *J. Geophys. Res.*, *82*, 2981–2987, doi:10.1029/JB082i020p02981.

King, C. Y., R. D. Nason, and D. Tocher (1973), Kinematics of fault creep, *Philos. Trans. R. Soc. London, Ser. A*, *274*, 355–360, doi:10.1098/rsta.1973.0063.

Klinger, R. E., and T. K. Rockwell (1989), Flexural-slip folding along the eastern Elmore Ranch fault in the Superstition Hills earthquake sequence of November 1987, *Bull. Seismol. Soc. Am.*, *79*, 297–303.

Kohler, W. M., and G. S. Fuis (1986), Travel-time, time-term, and basement depth maps for the Imperial-Valley region, California, from explosions, *Bull. Seismol. Soc. Am.*, *76*, 1289–1303.

Lienkaemper, J. J., B. Baker, and F. S. McFarland (2006), Surface slip associated with the 2004 Parkfield, California, earthquake measured on alinement arrays, *Bull. Seismol. Soc. Am.*, *96*(4B), S239–S249, doi:10.1785/0120050806.

Lin, G. Q., P. M. Shearer, and E. Hauksson (2007), Applying a three-dimensional velocity model, waveform cross correlation, and cluster analysis to locate southern California seismicity from 1981 to 2005, *J. Geophys. Res.*, *112*, B12309, doi:10.1029/2007JB004986.

Lindvall, S. C., T. K. Rockwell, and K. W. Hudnut (1989), Evidence for prehistoric earthquakes on the Superstition Hills fault from offset geomorphic features, *Bull. Seismol. Soc. Am.*, *79*, 342–361.

Lorenzetti, E., and T. E. Tullis (1989), Geodetic predictions of a strike slip fault model: Implications for intermediate-term and short-term earthquake prediction, *J. Geophys. Res.*, *94*, 12,343–12,361, doi:10.1029/JB094iB09p12343.

Louie, J. N., C. R. Allen, D. C. Johnson, P. C. Haase, and S. N. Cohn (1985), Fault slip in southern California, *Bull. Seismol. Soc. Am.*, *75*, 811–833.

Lyons, S., and D. Sandwell (2003), Fault creep along the southern San Andreas from interferometric synthetic aperture radar, permanent scatterers, and stacking, *J. Geophys. Res.*, *108*(B1), 2047, doi:10.1029/2002JB001831.

Lyons, S. N., Y. Bock, and D. T. Sandwell (2002), Creep along the imperial fault, southern California, from GPS measurements, *J. Geophys. Res.*, *107*(B10), 2249, doi:10.1029/2001JB000763.

Malservisi, R., K. P. Furlong, and C. R. Gans (2005), Microseismicity and creeping faults: Hints from modeling the Hayward fault, California (USA), *Earth Planet. Sci. Lett.*, *234*, 421–435, doi:10.1016/j.epsl.2005.02.039.

Marone, C., and C. H. Scholz (1988), The depth of seismic faulting and the upper transition from stable to unstable slip regimes, *Geophys. Res. Lett.*, *15*, 621–624, doi:10.1029/GL015i006p00621.

Marone, C. J., C. H. Scholtz, and R. Bilham (1991), On the mechanics of earthquake afterslip, *J. Geophys. Res.*, *96*, 8441–8452, doi:10.1029/91JB00275.

Massonnet, D., and K. L. Feigl (1998), Radar interferometry and its application to changes in the Earth's surface, *Rev. Geophys.*, *36*, 441–500, doi:10.1029/97RG03139.

Mavko, G. M. (1982), Fault interaction near Hollister, California, *J. Geophys. Res.*, *87*, 7807–7816, doi:10.1029/JB087iB09p07807.

Mcgill, S. F., C. R. Allen, K. W. Hudnut, D. C. Johnson, W. F. Miller, and K. E. Sieh (1989), Slip on the Superstition Hills fault and on nearby faults associated with the 24 November 1987 Elmore Ranch and Superstition Hills earthquakes, southern California, *Bull. Seismol. Soc. Am.*, *79*, 362–375.

Mellors, R. J., and A. Boisvert (2003), Deformation near the Coyote Creek fault, Imperial County, California: Tectonic or groundwater-related?, *Geochem. Geophys. Geosyst.*, *4*(2), 1012, doi:10.1029/2001GC000254.

Murray, J., and P. Segall (2002), Testing time-predictable earthquake recurrence by direct measurement of strain accumulation and release, *Nature*, *419*, 287–291, doi:10.1038/nature00984.

Nason, R. D. (1971), Investigation of fault creep slippage in northern and central California, Ph.D. thesis, Univ. of Calif., San Diego.

Nielsen, S., L. Knopoff, and A. Tarantola (1995), Model of earthquake recurrence: Role of elastic-wave radiation, relaxation of friction, and inhomogeneity, *J. Geophys. Res.*, *100*, 12,423–12,430, doi:10.1029/95JB00714.

Okada, Y. (1985), Surface deformation due to shear and tensile faults in a half-space, *Bull. Seismol. Soc. Am.*, *75*, 1135–1154.

Parker, R. L. (1977), Understanding inverse theory, *Annu. Rev. Earth Planet. Sci.*, *5*, 35–64, doi:10.1146/annurev.ea.05.050177.000343.

Parker, R. L., and Y. Q. Song (2005), Assigning uncertainties in the inversion of NMR relaxation data, *J. Magn. Reson.*, *174*, 314–324, doi:10.1016/j.jmr.2005.03.002.

Prescott, W. H., M. Lisowski, and J. C. Savage (1981), Geodetic measurement of crustal deformation on the San Andreas, Hayward, and Calaveras faults near San Francisco, California, *J. Geophys. Res.*, *86*, 853–869.

Rice, J. R., N. Lapustaa, and K. Ranjitha (2001), Rate and state dependent friction and the stability of sliding between elastically deformable solids, *J. Mech. Phys. Solids*, *49*, 1865–1898, doi:10.1016/S0022-5096(01)00042-4.

Rosen, P. A., S. Hensley, H. A. Zebker, F. H. Webb, and E. J. Fielding (1996), Surface deformation and coherence measurements of Kilauea volcano, Hawaii, from SIR-C radar interferometry, *J. Geophys. Res.*, *101*, 23,109–23,125, doi:10.1029/96JE01459.

Rymer, M. J., J. Boatwright, L. C. Seekins, J. D. Yule, and J. Liu (2002), Triggered surface slips in the Salton Trough associated with the 1999 Hector Mine, California, earthquake, *Bull. Seismol. Soc. Am.*, *92*, 1300–1317, doi:10.1785/0120000935.

Savage, J. C. (2006), Dislocation pileup as a representation of strain accumulation on a strike-slip fault, *J. Geophys. Res.*, *111*, B04405, doi:10.1029/2005JB004021.

Savage, J. C., and M. Lisowski (1993), Inferred depth of creep on the Hayward fault, central California, *J. Geophys. Res.*, *98*, 787–793, doi:10.1029/92JB01871.

Savage, J. C., W. H. Prescott, M. Lisowski, and N. E. King (1981), Strain accumulation in southern California, 1973–1980, *J. Geophys. Res.*, *86*, 6991–7001, doi:10.1029/JB086iB08p06991.

Schmidt, D. A., R. Burgmann, R. M. Nadeau, and D. d'Alessio (2005), Distribution of aseismic slip rate on the Hayward fault inferred from seismic and geodetic data, *J. Geophys. Res.*, *110*, B08406, doi:10.1029/2004JB003397.

Schulz, S. S., G. M. Mavko, R. O. Burford, and W. D. Stuart (1982), Long-term fault creep observations in central California, *J. Geophys. Res.*, *87*, 6977–6982, doi:10.1029/JB087iB08p06977.

Sharp, R. V. (1989), Pre-earthquake displacement and triggered displacement on the Imperial fault associated with the Superstition Hills earthquake of 24 November 1987, *Bull. Seismol. Soc. Am.*, *79*, 466–479.

Sharp, R. V., and J. L. Saxton (1989), 3-dimensional records of surface displacement on the Superstition Hills fault zone associated with the earthquakes of 24 November 1987, *Bull. Seismol. Soc. Am.*, *79*, 376–389.

Sharp, R. V., et al. (1989), Surface faulting along the Superstition Hills fault zone and nearby faults associated with the earthquakes of 24 November 1987, *Bull. Seismol. Soc. Am.*, *79*, 252–281.

Shen, Z. K., D. D. Jackson, and B. X. Ge (1996), Crustal deformation across and beyond the Los Angeles basin from geodetic measurements, *J. Geophys. Res.*, *101*, 27,957–27,980, doi:10.1029/96JB02544.

Sieh, K. E., and P. L. Williams (1990), Behavior of the southernmost San Andreas Fault during the past 300 years, *J. Geophys. Res.*, *95*, 6629–6645, doi:10.1029/JB095iB05p06629.

Simpson, R. W., J. J. Lienkaemper, and J. S. Galehouse (2001), Variations in creep rate along the Hayward Fault, California, interpreted as changes in depth of creep, *Geophys. Res. Lett.*, *28*, 2269–2272, doi:10.1029/2001GL012979.

Steinbrugge, K. V., and E. G. Zacher (1960), Creep on the San Andreas Fault: Fault creep and property damage, *Bull. Seismol. Soc. Am.*, *50*, 389–396.

Thatcher, W. (1990), Order and diversity in the modes of circum-Pacific earthquake recurrence, *J. Geophys. Res.*, *95*, 2609–2623, doi:10.1029/JB095iB03p02609.

Tocher, D. (1960), Creep on the San Andreas Fault: Creep rate and related measurements at Vineyard, California, *Bull. Seismol. Soc. Am.*, *50*, 396–404.

Toda, S., and R. S. Stein (2002), Response of the San Andreas fault to the 1983 Coalinga-Nunez earthquakes: An application of interaction-based probabilities for Parkfield, *J. Geophys. Res.*, *107*(B6), 2126, doi:10.1029/2001JB000172.

Wang, R. J., F. L. Martin, and F. Roth (2003), Computation of deformation induced by earthquakes in a multi-layered elastic crust—FORTRAN programs EDGRN/EDCMP, *Comput. Geosci.*, *29*, 195–207, doi:10.1016/S0098-3004(02)00111-5.

Weertman, J. (1965), Relationship between displacements on a free surface and the stress on a fault, *Bull. Seismol. Soc. Am.*, *55*, 945–953.

Wennerberg, L., and R. V. Sharp (1997), Bulk-friction modeling of afterslip and the modified Omori law, *Tectonophysics*, *277*, 109–136, doi:10.1016/S0040-1951(97)00081-4.

Wesson, R. L. (1988), Dynamics of fault creep, *J. Geophys. Res.*, *93*, 8929–8951, doi:10.1029/JB093iB08p08929.

Williams, P. L., and H. W. Magistrale (1989), Slip along the Superstition Hills fault associated with the 24 November 1987 Superstition Hills, California, earthquake, *Bull. Seismol. Soc. Am.*, *79*, 390–410.

Wyss, M. (2001), Locked and creeping patches along the Hayward fault, California, *Geophys. Res. Lett.*, *28*, 3537–3540, doi:10.1029/2001GL013499.

---

Y. Fialko, D. Sandwell, and M. Wei, Institute of Geophysics and Planetary Physics, Scripps Institution of Oceanography, University of California, San Diego, 9500 Gilman Drive, La Jolla, CA 92093-0225, USA. (mwei@ucsd.edu)